
PARTICLE-BASED ADAPTIVE DISCRETIZATION FOR CONTINUOUS CONTROL USING DEEP REINFORCEMENT LEARNING

Pei Xu

School of Computing
Clemson University
peix@clemson.edu

Ioannis Karamouzas

School of Computing
Clemson University
ioannis@clemson.edu

ABSTRACT

Learning controls in high-dimensional continuous action spaces, such as controlling the movements of highly articulated agents and robots, has long been a standing challenge to model-free deep reinforcement learning (DRL). In this paper we propose a general, yet simple, framework for improving the action exploration of policy gradient DRL algorithms. Our approach adapts ideas from the particle filtering literature to dynamically discretize the continuous action space and track policies represented as a mixture of Gaussians. We demonstrate the applicability of our approach on state-of-the-art DRL baselines in challenging high-dimensional motor tasks involving articulated agents. We show that our adaptive particle-based discretization leads to improved final performance and speed of convergence as compared to uniform discretization schemes and to corresponding implementations in continuous action spaces, highlighting the importance of exploration. In addition, the resulting policies are more stable, exhibiting less variance across different training trials.

1 Introduction

Recently, the rise of deep learning combined with advances in CPU and GPU hardware has renewed the interest in model-free reinforcement learning, enabling agents to learn policies from raw observation data through interactions with the environment. In the last few years, impressive results have been obtained by deep reinforcement learning (DRL) both on physical and simulated articulated agents for a wide range of motor tasks that involve learning controls in high-dimensional continuous action spaces [1, 2, 3, 4]. Despite recent success, though, state-of-the-art model-free DRL algorithms for continuous control problems still require a large amount of training samples and computation. Due to the infinite feasible action choices, controlling many degrees of freedom (DOFs) is inherently ambiguous with respect to most behaviors, resulting in challenging control problems that are under specified and highly dimensional. Even though such issues can be mitigated by tracking reference data or using expert data to bootstrap training [5, 6, 7, 8], in many cases we may not have access to such data. Even if we have a fine-tuned reward function designed according to expert data, the question of how to sufficiently and efficiently explore the high-dimensional action spaces to improve sampling and training time efficiency still exists.

In general, on-policy DRL methods such as PPO [9], TRPO [10], and A3C [11] can become prohibitively expensive for continuous control problems given the huge number of training samples needed to learn a policy in high-dimensional action spaces. On the other hand, off-policy methods exhibit better sample efficiency as they can reuse past experiences. While the widely used off-policy method Deep Q-Network (DQN) only works for discrete action spaces, algorithms like DDPG [1] and SVG(0) [12] are very popular for continuous control problems, as they use a separate actor network and exploit policy gradient to directly search policies in the continuous action space. However, such approaches can be too sensitive to the selected hyperparameters, often yielding to unstable policies [13]

Regardless if on-policy or off-policy learning is employed, ideally we want to keep trying multiple actions until we are confident about the best one(s). However, DRL algorithms for continuous control problems typically employ an independent multivariate Gaussian as the policy distribution, which is unimodal and can prematurely commit to suboptimal controls [14]. Consider, for example, an articulated agent that needs to learn a mapping from states to actions based on all individual joints. This is a very challenging task as for a given DOF and a continuous

action space, we need to find a state-dependent mean and standard deviation. And of course the problem becomes even more complicated as we need to do the same thing for all DOFs and determine how they work in synchrony for a given state. To address such issues researchers have been investigating hierarchical policies for structured exploration [15, 16, 17, 18]. In addition, entropy-regularized DRL methods recently have gained a lot of popularity focusing on optimizing both the expected cumulative reward and the expected entropy of the policies to help action exploration. Earlier maximum entropy approaches utilized discrete multinomial policies, Gaussian policies, and more generic energy-based functions [19, 20, 21, 22, 14]. More recently, an off-policy soft actor-critic algorithm (SAC) based on maximum entropy has been proposed, which shows sampling efficiency and outperforms other state-of-the-art off-policy and on-policy approaches, such as DDPG and PPO, in many benchmarks [23]. SAC was further revised in [24] to have a simpler architecture and better stability.

Despite such advancements, though, and given the large amount of computation resources needed by the physics simulation and/or the high cost for training on real robots, the requirement of efficient sampling still poses a serious challenge in the application of DRL to robot and character control problems. As such, recent work has also focused on the idea of discretizing the action space for continuous control problems. While the combination of distinct actions increases exponentially as the number of action dimensions increases and thus prevents the application of DQN in high-dimension control problems, the joint categorical distributions can become tractable if factorization is employed. For example, PPO with categorical distributions defined in a discretized action space has been successfully exploited to learn manipulation policies for a 24-DOF robotic hand [25] and locomotion policies for a high-dimensional musculoskeletal human model [26]. An intuitive explanation behind such a success is that discretization can largely reduce the size of the action spaces, which would make it easier to find an optimal solution from all feasible actions. Indeed, the recent work in [27] has shown that action discretization is a simple yet powerful technique for on-policy optimization. Though, as samples are drawn only from some small number of fixed locations in each action dimension, the robustness and effectiveness of such discretization schemes may vary depending on the task. Furthermore, categorical distributions cannot be extended to off-policy frameworks, like DDPG and SAC, as they are not differentiable.

In this paper, we propose a general solution for improving the exploration of high dimensional action spaces during training of policy gradient algorithms. Our approach relies on the discretization of the action space. However, in contrast to the prior discretization technique that uses a categorical distribution per action dimension, we represent a policy as a mixture of Gaussians. In addition, instead of discretizing the action space by a fixed set of action choices, we exploit a particle filtering approach to adaptively discretize the action space and track the posterior policy distribution during training. The resulting network, which we call particle filter policy network (PFPN), is suitable for both on-policy and off-policy policy gradient methods. We evaluate PFPN on state-of-the-art baselines including the recent SAC, IMPALA [28], PPO, and A2C/A3C, using challenging high-dimensional tasks from the Roboschool suite [10] and the DeepMimic framework [5]. We show that our particle-based adaptive discretization exhibits better performance compared to the fixed, uniform discretization scheme and to corresponding implementations in continuous action spaces, highlighting its sample efficiency and stability.

2 Background

2.1 Policy Gradient Method

We consider a standard reinforcement learning setup where given a time horizon H and the trajectory $\tau = (s_1, \mathbf{a}_1, \dots, s_H, \mathbf{a}_H)$ obtained by a parameterized policy π_θ , with s_t and \mathbf{a}_t denoting the state and action taken at time step t , respectively, the goal is to learn the parameters θ that maximize the agent’s cumulative reward:

$$J(\theta) = \mathbb{E}_{\tau \sim p_\theta(\tau)} \left[\sum_{t=1}^H r_t(\tau) \right] = \int p_\theta(\tau) r(\tau) d\tau. \quad (1)$$

Here, $p_\theta(\tau) = \sum_t \pi_\theta(\mathbf{a}|s)$ denotes the state-action visitation distribution for the trajectory τ induced by the policy π_θ , and $r(\tau) = \sum_t r(s_t, \mathbf{a}_t)$ where $r(s_t, \mathbf{a}_t)$ is the reward received at time t .

We can maximize $J(\theta)$ by adjusting the policy parameters θ through the gradient ascent method, where the gradient of the expected reward can be determined according to the policy gradient theorem [29]:

$$\nabla_\theta J(\theta) = \mathbb{E}_{a_t \sim \pi_\theta(\cdot|s_t)} \left[\sum_t r(s_t, a_t) \nabla_\theta \log \pi_\theta(a_t|s_t) | s_t \right] \quad (2)$$

In order to reduce the variance of the policy gradient estimate, the estimate of the Q-value provided by the cumulative reward along the trajectory can be improved by replacing it with any unbiased or more stable estimator such as

the Q-value with discount factor, the advantage or generalized advantage estimation [30], or that with importance sampling [9]. For simplicity, we use A_t to denote any kind of estimators. Some of the estimators need a baseline subtraction to further reduce variance and improve stability. A typically used baseline is the state-value function $V(s_t) := \mathbb{E}_{a \sim \pi(\cdot|s_t)} [\sum_t r(s_t, a) + V(s_{t+1})]$. In DRL, the value function can be approximated by a separate network (critic) that is updated in tandem with the policy network (actor). This gives rise to a family of policy gradient algorithms known as actor-critic.

On-Policy and Off-Policy Actor-Critics. In on-policy learning, the update policy is also the behavior policy based on which a trajectory is obtained to estimate A_t . Common on-policy actor-critic methods include A2C/A3C [11], and PPO [9]. In off-policy learning, typically, the model directly learns to estimate A_t given a state-action pair such that policy can be updated without the knowledge of a whole trajectory. This results in more sample efficient approaches as samples can be reused. Common off-policy actor-critic methods include DDPG [1] and SAC [23], where their critic network is used to predict the Q- and soft Q-value, respectively. The actor network in such methods is optimized directly by maximizing the Q-value [31] or soft Q-value [23], resulting in the following policy gradient for SAC:

$$\nabla_{\theta} J(\theta) = \nabla_{\theta} \mathbb{E}_{s_t \sim \mathcal{B}} [\log \pi_{\theta}(\mathbf{a}_t | s_t) - Q_s(s_t, \mathbf{a}_t | s_t)] \quad (3)$$

where \mathcal{B} denotes a replay buffer of the collected samples, and $Q_s(s_t, a_t)$ is the soft Q-value and $\mathbf{a}_t := f_{\theta}(\epsilon, s_t)$ is a differentiable sampling result with noise ϵ .

2.2 Policy Representation

Given a multi-dimensional continuous action space, the most common choice is to model the policy π_{θ} as a multivariate Gaussian distribution with independent components for each action dimension. For simplicity, we consider a_t for the case with only one dimension and has policy $\pi_{\theta}(a_t | s_t) := \mathcal{N}(\mu_{\theta}, \sigma_{\theta}^2)$. Then, we can obtain

$$\log \pi_{\theta}(a_t | s_t) = -\frac{(a_t - \mu_{\theta}(s_t))^2}{2\sigma_{\theta}^2(s_t)} - \log \sigma_{\theta}(s_t) - c, \quad (4)$$

where $c = \log 2\pi$ is a constant.

Given a sampled action a_t and the estimate of cumulative rewards A_t , the optimization process, based on the above expression, can be imagined as that of shifting $\mu(s_t)$ towards the direction of a_t if A_t is higher than the expectation, or to the opposite direction if A_t is smaller. Such an approach, though, can easily converge to a suboptimal solution, if there is a low reward distribution much wider than $\sigma_{\theta}(s_t)$ between the current location of $\mu(s_t)$ and the optimal solution, or hard to be optimized if the reward landscape is the same around $\mu(s_t)$. These issues arise due to the fact that Gaussian distributions are inherently unimodal [14]. Sampling happens only around the mean value of the distribution and the exploration ability depends on the standard deviation. A large standard deviation may promote exploration but may also slow down the convergence. And, as long as the optimization process is going to converge, the standard deviation will unavoidably decrease, but this may happen prematurely before sampling from a better region.

3 Particle Filter Policy Network

In this section, we describe our Particle Filter Policy Network algorithm that addresses the unimodality issues from which typical Gaussian-based policy networks suffer. To do so, we draw inspiration from the particle filter literature [32] and in particular the sequential importance resampling (SIR) approach [33, 34]. Our approach adaptively discretizes the action space, by using state-independent particles, each capturing a Gaussian distribution. Thus, the policy network, instead of directly generating actions, it is tasked with choosing particles, while the final actions are generated by sampling from the selected particles. Next, we first define action policies based on particles, and then focus on the training of our policy network. We also refer the reader to Appendix A for a brief introduction on SIR and the close connection of our approach to it.

3.1 Particle-based Action Policy

Let $\mathcal{P} := \{p_{i,k}, w_{i,k}\}$, be a weighted set of particles where $p_{i,k} = \mathcal{N}(\mu_{i,k}, \sigma_{i,k}^2)$ is the i -th particle on the k -th action dimension that represents a univariate Gaussian distribution, and $w_{i,k}$ denotes the corresponding weight of the particle. Given \mathcal{P} , we define the policy as

$$\pi_{\theta}^{\mathcal{P}}(\mathbf{a}_t | s_t) = \prod_k \sum_i w_{i,k}(s_t | \theta) p_{i,k}(a_{t,k} | \mu_{i,k}, \sigma_{i,k}) \quad (5)$$

where $a_{t,k} \in \mathbf{a}_t$ is the sampled action at the time step t for the action dimension k , and $w_{i,k}(\cdot|\theta)$ is the direct output of the policy network after softmax operation over the output neurons for the k -th dimension satisfying $\sum_i w_{i,k} = 1$.

While the softmax operation gives us a categorical distribution defined by $w_{\cdot,k}$, the nature of the policy for each dimension is a mixture of Gaussian distributions. Given sufficient component distributions, it can approximate arbitrary smooth density. Sampling through the mixture of Gaussians can be done by two steps. First, we perform sampling on the categorical distribution to choose a particle, j , for each dimension, k , based on the weights

$$j(\mathbf{s}_t) \sim P(\cdot|w_{\cdot,k}(\mathbf{s}_t)). \quad (6)$$

Then, we can draw samples from the Gaussian distribution represented by the chosen particles

$$a_{t,k} \sim p_{j,k(\mathbf{s}_t)}(\cdot|\mu_{j,k(\mathbf{s}_t)}, \sigma_{j,k(\mathbf{s}_t)}). \quad (7)$$

Sampling through the weighted particles is stratified, which is considered optimal in terms of variance [35]. By stratified sampling, given a state, action exploration could occur at several different locations in the action space and weightedly to fit the diversity distribution of the cumulative reward or its estimator, instead of being uniformly or only near one single location.

Some algorithms, like A3C and IMPALA, often introduce differential entropy loss to encourage exploration. However, it is not feasible to analytically evaluate the differential entropy of a mixture of Gaussians without approximation [36]. Instead, we use the entropy of the categorical distribution if a differential entropy term is needed during optimization to encourage action exploration.

3.2 Training

The proposed particle-based policy distribution is general and can be applied directly to any algorithm using the policy gradient method with Equation 2. To initialize the training, due to lack of prior knowledge, the particles can be distributed uniformly along the action dimensions. Without loss of generality, let us consider below only one action dimension and drop the subscript k . Then, at each training step, each particle, p_i , will move along the action dimension on which it is defined and be updated by

$$\begin{aligned} \nabla J(\mu_i, \sigma_i) &= \mathbb{E} \left[\sum_t A_t \nabla_{\mu_i} \log \sum_i w_i(\mathbf{s}_t|\theta) p_i(a_t|\mu_i, \sigma_i) | \mathbf{s}_t \right] \\ &= \mathbb{E} \left[\sum_t c_t w_i(\mathbf{s}_t|\theta) \nabla_{\mu_i} p_i(a_t|\mu_i, \sigma_i) | \mathbf{s}_t \right] \end{aligned} \quad (8)$$

where $a_t \sim \pi_{\theta, \mathcal{P}}(\cdot|\mathbf{s}_t)$ is the actions chosen during sampling, A_t is the estimator of the cumulative $r(\cdot, \cdot)$ term in Equation 2 and

$$c_t = \frac{A_t}{\sum_i w_i(\mathbf{s}_t|\theta) p_i(a_t|\mu_i, \sigma_i)} \quad (9)$$

is a coefficient shared by all particles on the same action dimension. Similarly, for the update of the neural network, we have

$$\nabla J(\theta) = \mathbb{E} \left[\sum_t c_t p_i(a_t|\mu_i, \sigma_i) \nabla_{\theta} w_i(\mathbf{s}_t|\theta) | \mathbf{s}_t \right] \quad (10)$$

Although sampling is performed on only one particle for each dimension, all the dimension's particles will be updated during each iteration of the training to move towards or away of the location of a_t according to A_t . The amount of the update, however, is regulated by the state-dependent weight $w_i(\mathbf{s}_t|\theta)$: particles that have small probabilities to be chosen for a given state \mathbf{s}_t will be considered as uninteresting and be barely updated or not be updated at all depending on their associated weights. On the other hand, the contribution of weights is limited by the distance between a particle and the sampled action. In practice, a distance of six times the standard deviation to a sampled action is far enough to prevent that particles from moving as well as from boosting the associated weighted. In summary, the action policy performs optimization only for those "interesting" particles and helps avoid converging all particles to a single average global optimal location over all states.

Using the above process, particles can converge to different optimal locations near it as training goes on. They would be distributed multimodally according to A_t , rather than collapse to a unimodal, Gaussian-like distribution. This results in an adaptive discretization scheme of the action space that is state-independent.

3.3 Resampling

Similar to traditional particle filtering approaches, our approach would encounter the problem of degeneracy [37]. During training, a particle placed near a location at which sampling gives a low A_t value would achieve a low weight gain and its associated weight may keep decreasing. Once the weight reaches near zero, the particle will not be updated anymore by training through gradient and become ‘dead’. To address this problem, we borrow the idea of importance resampling from particle filters, but we do not resample the entire set of particles. Because particle weights in our approach are state-dependent, equalizing the weights after resampling will make it unable to trace interesting particles defined with respect to a given state. Instead, we perform resampling only for dead particles and reactivate them by duplicating some better, alive target particles.

A particle can be considered dead if its maximum weight for all possible states is too small, i.e.

$$\max_{s_t} w_i(s_t|\theta) < \epsilon \quad (11)$$

where ϵ is a small positive threshold number. In practice, we cannot really check $w_i(s_t|\theta)$ for all the possible states, but can keep tracking it during sampling.

The target particle τ_i is drawn for each dead particle i independently from the categorical distribution weighted with the average weight of each particle during some sampling episodes, i.e.

$$\tau_i \sim P(\cdot | \mathbb{E}_{s_t} [w_k(s_t|\theta)], k = 1, 2, \dots) \quad (12)$$

Because the target particle is drawn with randomness and independently for each dead ones, it may happen that several dead particles share the same target particle. Let \mathcal{D}_τ be a set of dead particles sharing the same target particle τ . Given Equations 11 and 12, if ϵ is small enough, we have $\tau \notin \mathcal{D}_k$ for any dead particle set \mathcal{D}_k .

Resampling makes the dead particles be a duplicate of the target one. After resampling, the target particle τ and any particle $s \in \mathcal{D}_\tau$ should share the same logits L'_τ leading to the same weight. Whereas the neural network outputs unnormalized logits before the softmax operation, in order to make the weights after softmax unchanged for all other particles, we must ensure that the exponential sum of the logits for all particles is identical before and after resampling. That is to say, it must be satisfied that

$$\sum_{s \in \mathcal{D}_\tau} e^{L_s} + e^{L_\tau} = (|\mathcal{D}_\tau| + 1) e^{L'_\tau} \quad (13)$$

Assuming a fully connected layer is used to generate unnormalized logits in the policy network, the logits for the i -th particle are given by:

$$L_i(s_t) = \sum_k h_k(s_t) \omega_{k,i} + b_i, \quad (14)$$

where $h_k(s_t)$ is the hidden neuron output fed into the fully connected layer, $\omega_{k,i}$ and b_i are respectively the weight and bias parameters of that layer. Therefore, when duplicating the target particle τ , the weights of the reactivated particles $s \in \mathcal{D}_\tau$ can be equalized by directly copying $\omega_{\cdot,\tau}$ to $\omega_{\cdot,s}$ but applying an error correction term when synchronizing the bias parameters, i.e.

$$b_i \leftarrow b_\tau - \log(|\mathcal{D}_\tau| + 1) \quad (15)$$

where $i \in \mathcal{D} \cup \{\tau\}$. We refer the reader to the Appendix B for the inference of the error correction term.

A problem of resampling via duplicating is that it induces loss of diversity. If two particles are exactly the same, they will always be updated together at the same pace during training. To address this issue and benefit the action exploration, we add some regularization noise to the mean value when performing resampling for a dead particle such that the dead particle is resampled near the target one instead of being an exact copy of the target particle, i.e.

$$\sigma_i \leftarrow \sigma_\tau; \quad \mu_s \leftarrow \mu_\tau + \varepsilon_s \quad (16)$$

where $\varepsilon_s = \alpha_s \sigma_\tau + \text{SIGN}(\alpha_s) c$, $\alpha_s \sim U(-1, 1)$ is a random number and c is a constant positive number to prevent μ_s from being too close to μ_τ .

An overview of our Particle Filter Policy Network using resampling is provided in Algorithm 1. At each training step, each particle is updated and moves along its action dimension, while we also update accordingly the parameters of the policy network. To avoid the particle degeneracy problem, deprived particles are resampled every fixed number of environment steps. It should be noted that in the above we assume that each particle denotes a univariate Gaussian distribution over a single action dimension. However, our algorithm is also applicable to particles representing multivariate Gaussian distributions defined over the whole or a subspace of the entire action space.

Algorithm 1 DRL using Particle Filter Policy Network

```

Initialize the neural network parameter  $\theta$  and learning rate  $\alpha$ ;
initialize particle parameters  $\mu_i$  and  $\sigma_i$  to uniformly distribute particles on the target action dimension;
initialize the threshold  $\epsilon$  to detect dead particles using a small number.
loop
  for each environment step do
    Record the weight while sampling  $a_t \sim \pi_{\theta, \mathcal{P}}(\cdot | s_t)$ ,
     $\mathcal{W}_i \leftarrow \mathcal{W}_i \cup \{w_i(s_t | \theta)\}$ 
  end for
  for each training step do
     $\langle \mu_i, \sigma_i \rangle \leftarrow \langle \mu_i, \sigma_i \rangle + \alpha \nabla J(\mu_i, \sigma_i)$ 
     $\theta \leftarrow \theta + \alpha \nabla J(\theta)$ 
  end for
  for every  $n$  environment steps do
    for each particle  $i$  do
      if  $\max_{w_i \in \mathcal{W}_i} w_i < \epsilon$  then
         $\tau_i \sim P(\cdot | \mathbb{E}[w_k | w_k \in \mathcal{W}_k], k = 1, 2, \dots)$ 
         $\mathcal{T} \leftarrow \mathcal{T} \cup \{\tau_i\}, \mathcal{D}_{\tau_i} \leftarrow \mathcal{D}_{\tau_i} \cup \{i\}$ 
      end if
    end for
    for each target particle  $\tau \in \mathcal{T}$  do
      for each dead particle  $i \in \mathcal{D}_{\tau}$  do
         $\mu_i \leftarrow \mu_{\tau} + \varepsilon_i, \sigma_i \leftarrow \sigma_{\tau}, \omega_{\cdot, i} \leftarrow \omega_{\cdot, \tau}$ 
         $b_i \leftarrow b_{\tau} - \log(|\mathcal{D}_{\tau}| + 1)$ 
      end for
       $b_{\tau} \leftarrow b_{\tau} - \log(|\mathcal{D}_{\tau}| + 1)$ 
       $\mathcal{D}_{\tau} \leftarrow \emptyset$ 
    end for
     $\mathcal{T} \leftarrow \emptyset, \mathcal{W}_i \leftarrow \emptyset$ 
  end for
end loop
    
```

3.4 Differentiability Trick

The two-step sampling method described in Section 3.1 is indifferentiable, because of the standard way of sampling from the categorical distribution through which Gaussians are mixed. To address this issue, we consider the concrete distribution [38, 39] that generates a re-parameterized, differential continuous approximation to a categorical distribution. Given that $\mathbf{x} \sim \text{CONCRETE}(\{w_k(s_t | \theta); k = 1, 2, \dots\}, \cdot)$ is a differentiable sampling result approximating the categorical distribution defined by $w_k(s_t | \theta)$, we apply the Gumbel-softmax trick [40] to generate a differentiable sampling result form a mixture of Gaussians, $\sum_i w_i(s_t | \theta) \mathcal{N}(\mu_i, \sigma_i^2)$:

$$a_{\theta, \mathcal{P}}(\varepsilon, s_t) = \sum_i (\mu_i + \varepsilon_i \sigma_i) (x_i + \text{STOP}(\delta(i, \arg \max \mathbf{x}) - x_i)) \quad (17)$$

where $\varepsilon_i \sim \mathcal{N}(0, 1)$, $x_i \in \mathbf{x}$, $\text{STOP}(\cdot)$ is a “gradient stop” operation and $\delta(\cdot, \cdot)$ denotes the Kronecker delta function. By this reparameterization trick, the proposed action policy can be used in Q-value based off-policy algorithms, like SAC and DDPG.

4 Related Work

Our approach is closely related to approaches that rely on the discretization of the action space. While DQN-like approaches are very efficient [11] for problems with discrete action spaces, such techniques cannot scale well to high-dimensional action spaces due to the curse of dimensionality. Recently, [41] show their work to solve this issue by a sequential model and apply it on continuous control problems with discretized action spaces.

On the other hand, action discretization of high-dimensional control spaces has been successfully applied to policy gradient methods in order to improve sampling efficiency or training performance. A typical approach to overcome the explosion of the action space is to model each action dimension using a categorical distribution. In [25], for example, a

robot hand with 24 DOF was trained using a 11-bin, uniformly discretized action space. The work in [27] provides a series of benchmarks to compare the performance difference between continuous action spaces and discretized ones. All of such works focus on on-policy actor-critic algorithms using policy gradient methods and discretize the action space uniformly and with quite a few number of bins. While impressive results have been obtained that allow for better performance, such a uniform discretization approach heavily relies on the choice of candidate locations to find a good solution. As the action locations remain fixed, a number of futile locations may impede finding the optimal action. Indeed, as we show in Section 5.2, changing the number of bins can have a drastic impact on the asymptotic performance which can render such solutions rather unstable.

To address these issues, we proposed an adaptive discretization scheme of the action space based on particles. A similar idea was recently explored in [42] where a particle-based implementation of SAC was proposed. However, they optimize all particles together without importance weights, which results in the particles quickly collapsing to an average optimal location over all states. The completely state-independent particle definition makes the algorithm lose entropy regularization, and thus the resulting performance tends to be inferior to the vanilla SAC.

5 Experiments

The goal of our experiments is to evaluate whether adaptive discretization can promote action exploration, and the effect that it has on the final performance as well as sample complexity of existing policy gradient algorithms. We are also interested in its stability given that many policy optimization methods can exhibit high variance across different training seeds. We tested the applicability of our particle-based policy network to a number of policy gradient algorithms using a range of continuous control tasks from the Roboschool benchmark suite [10]. We chose the Roboschool suite as its tasks are typically more challenging than the corresponding ones from the OpenAI gym benchmark suite [43] with most algorithms typically exhibiting relatively poor performance.

Besides different algorithms, our particle-based discretization is also indifferent to how the action space is parameterized. To highlight this we also consider several tasks from the DeepMimic framework [5] where a 36-dimensional humanoid learns a locomotion policy based on motion capture data. The Roboschool environment directly uses torques to control articulated agents, whereas DeepMimic learns target joint angles that are given as input to a stable proportional-derivative (PD) controller [44] after converted from axis-angle representations to quaternions.

The PD servo has to be called multiple times during a simulation step to generate torques applied to the humanoid model. Due to such frequent calls, the training of DeepMimic tasks can become quite expensive. Hence, the learning can significantly benefit from algorithms that are sample efficient and exhibit fast convergence.

We evaluate our approach on two policy gradient baselines: the advantage actor critic and its distributed version (A2C/A3C) [11], which is a widely-used on-policy method that is known though to suffer from stability issues; and the proximal policy optimization (PPO/DPPO) [9], which is a stable method that exhibits good performance. In Appendix D, we also provide results using the recently proposed soft actor-critic (SAC) [23], an off-policy entropy regularized method that achieves state-of-the-art performance in many tasks; and the importance weighted actor-learner architecture (IMPALA) with the V-trace off-policy correction algorithm [28], a hybrid actor-critic approach that is highly distributed. Finally, we have also included comparisons between our approach and the uniform discretization scheme where actions are sampled from categorical distributions.

5.1 PFPN vs. Gaussian Baselines

Figure 1 shows the cumulative rewards of evaluation rollouts during training for PPO/DPPO and A2C/A3C using both the default policy network that employs Gaussian policies and our Particle Filter Policy Network (PFPN). DPPO and A3C are deployed for complex tasks, HumanoidBulletEnv-v0, DeepMimicWalk, DeepMimicKick and DeepMimicPunch, to parallelize the training in order to increase training time efficiency. We train five trials of each of the two versions of a given baseline (with different random seeds that are the same across the PFPN and Gaussian versions) and perform ten evaluation rollouts every 1,000 training steps using deterministic actions, which is the exact mean value of Gaussian distributions exploited by the policy network without adding noise.

As it can be seen in the figure, our approach significantly improves the behavior of the two on-policy methods in all of the six benchmarks. In particular, PFPN increases the stability of A2C/A3C as well as its final performance in AntBulletEnv-v0 and HalfCheetahBulletEnv-v0. The same applies to the three DeepMimic tasks where A3C reaches a final performance comparable to that of DPPO. Similar to A2C/A3C, the PFPN version of PPO/DPPO is more stable and sampling efficient and exhibits higher asymptotic performance.

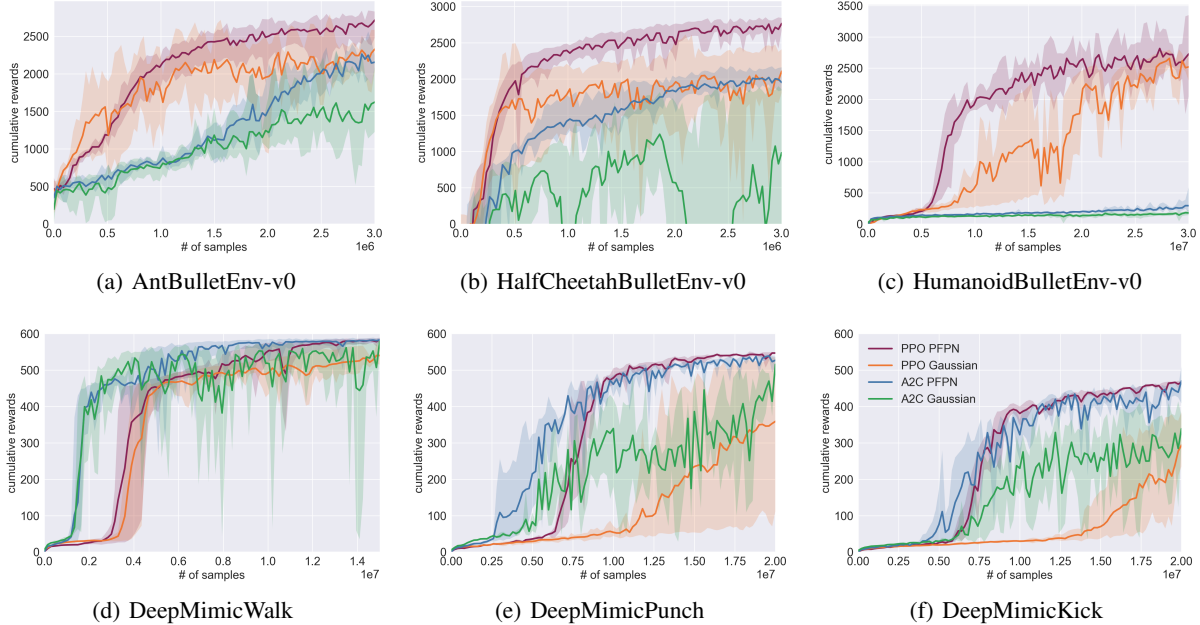


Figure 1: Performance of PPO/DPPO and A2C/A3C using Gaussian-based action policies and our proposed Particle Filter Policy Networks (PFPN). Solid lines report the average and shaded regions the minimum and maximum cumulative rewards achieved over five trials. In all benchmarks, PFPN outperforms Gaussian-based policies.

We refer to Appendix D for results obtained with SAC and IMPALA baselines and additional tasks, and to Appendix C for the hyperparameters employed in these benchmarks.

5.2 Ablation Study

Resampling Strategies. We tested PFPN with the default resampling strategy explained in Section 3.3, where a target particle is selected with a probability proportional to its weights, against a number of alternative strategies where an inactive particle resamples randomly from the top- $x\%$ of particles as ranked by their weights. We refer the reader to Appendix E for detailed results. In Figure 2, we show DPPO results on HumanoidBulletEnv-v0 and DeepMimicWalk using the default PFPN resampling strategy, PFPN with no resampling (top-0%), and PFPN that randomly resamples from all particles (top-100%). It can be seen that any resampling strategy, even a completely random one (top-100%) could help improve the final training performance compared to no resampling. However, random resampling could lead to high variance and make the training process unstable by introducing too much uncertainty, especially in the earlier stages of training where the particles have not converged yet to optimal locations. In contrast, the default resampling strategy that accounts for the importance weights of the particles is the most stable. Resampling from the top-1% of particles (see Appendix E) results in a strategy of duplicating always the best one. This could make too many particles redistributed just around one location and limit the benefit of action exploration brought by resampling.

Number of Particles. We analyze the effect that the number of particles have on the performance of the PFPN-baselines. While Table 1 gives us a simple image about this, the detailed results are shown in Appendix F. Even though for each baseline and task, the best final performance is obtained by different number of particles, we found that in practice, there is a wide range of particle numbers that work quite well in each task outperforming the traditional Gaussian-based policy networks. As such, we used the same values across all of the Roboschool and DeepMimic tasks, 35 and 100 particles respectively, as the default hyperparameters used in the baseline benchmarks.

Comparison to Uniform Discretization. Overall, compared to Gaussian-based policy networks, uniformly discretizing each action dimension and sampling actions from a categorical distribution can work quite well, as has been shown in recent prior work [27, 25]. However, as shown in Table 1, our adaptive, particle-based discretization outperforms the uniform discretization scheme, especially as the task complexity increases. In the more complex DeepMimic tasks, uniform discretization is significantly worse than PFPN both in terms of speed of learning and asymptotic performance,

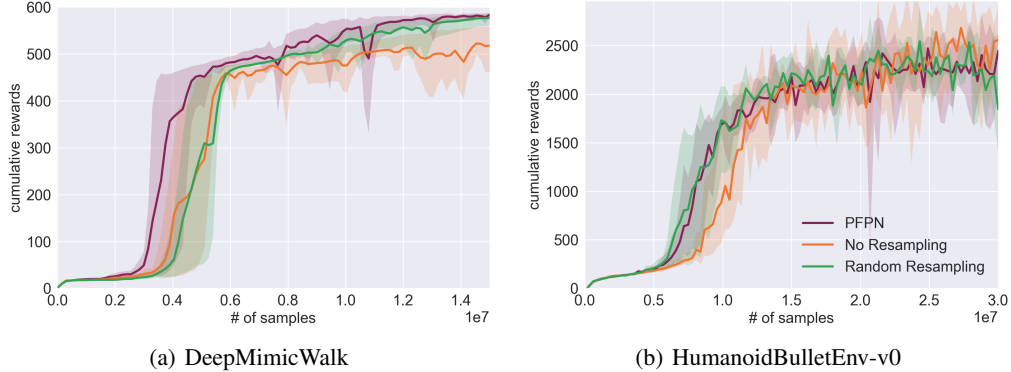


Figure 2: Performance of different resampling strategies on the Humanoid and DeepMimicWalk benchmarks using DPPO. We compare the default PFPN strategy, where the probability of drawing a target particle is proportional to its weight, to PFPN without resampling and PFPN that employs random resampling.

bins/ particles	AntBulletEnv-v0		HalfCheetahBulletEnv-v0		DeepMimicWalk	
	PFPN	DISCRETE	PFPN	DISCRETE	PFPN	DISCRETE
10	3059 \pm 223	2934 \pm 229	2825 \pm 208	2740 \pm 391	-	-
35	2714 \pm 124	2498 \pm 242	2764 \pm 68	2550 \pm 84	578 \pm 7	384 \pm 178
50	2617 \pm 221	2416 \pm 245	2414 \pm 281	2489 \pm 250	566 \pm 30	454 \pm 38
100	-	-	-	-	583 \pm 3	472 \pm 64
Gaussian	2328 \pm 199		2105 \pm 256		540 \pm 18	

Table 1: Comparison between Particle Filter Policy Network (PFPN) and uniform discretization (DISCRETE) on three benchmarks using PPO/DPPO while varying the resolution of each action dimension. PFPN exhibits the similar or significantly better performance than DISCRETE for a given resolution and benchmark, while being more stable across different resolutions within a benchmark. Reported numbers denote final performance averaged over 5 trials \pm the standard deviation.

while also exhibiting worse performance than the Gaussian-based policy networks. In addition, in DeepMimic, varying the number of bins per actions dimension can have a drastic impact on the sampling efficiency. In contrast, our approach stays much more stable as the number of particles changes. Finally, as the evaluation results reported in Table 1 are based on deterministic actions, PFPN’s performance clearly highlights the better quality of policies generated by an adaptive discretization scheme as compared to a uniform one.

We refer the reader to Appendix F for additional results regarding the sensitivity of PFPN to the number of particles used and for additional comparisons to uniform discretization.

6 Conclusion

We present a general approach for improving the action exploration of policy gradient DRL algorithms as well as a method to adaptively discretize continuous action space. Our approach replaces Gaussian policies that have been the staple for high-dimensional continuous control tasks with a collection of state-independent samples, each capturing a Gaussian distribution, that are updated analogously to particle filters. For tasks with continuous action spaces, our approach can be easily adopted in a DRL algorithm using policy gradient as a replacement of Gaussian or any other action policy without changing the algorithm itself. We empirically show that our particle filter policy network can add stability and significantly increase the performance and sampling efficiency of policy gradient methods especially in complex continuous tasks. In our current benchmarks, the same amount of particles are assigned to each action dimension. However, certain dimensions may need a higher resolution than others for a given motor task. Hence, we plan to investigate the use of different number of particles per action dimension. We also want to account for the synergy that exists between different action dimensions when articulated agents perform a task by assigning particles to multiple dimensions together, which opens an exciting avenue for future work.

References

- [1] Timothy P Lillicrap, Jonathan J Hunt, Alexander Pritzel, Nicolas Heess, Tom Erez, Yuval Tassa, David Silver, and Daan Wierstra. Continuous control with deep reinforcement learning. *arXiv preprint arXiv:1509.02971*, 2015.
- [2] Nicolas Heess, Srinivasan Sriram, Jay Lemmon, Josh Merel, Greg Wayne, Yuval Tassa, Tom Erez, Ziyu Wang, SM Eslami, Martin Riedmiller, et al. Emergence of locomotion behaviours in rich environments. *arXiv preprint arXiv:1707.02286*, 2017.
- [3] Tuomas Haarnoja, Aurick Zhou, Sehoon Ha, Jie Tan, George Tucker, and Sergey Levine. Learning to walk via deep reinforcement learning. In *Robotics: Science and Systems*, 2018.
- [4] Sergey Levine, Chelsea Finn, Trevor Darrell, and Pieter Abbeel. End-to-end training of deep visuomotor policies. *The Journal of Machine Learning Research*, 17(1):1334–1373, 2016.
- [5] Xue Bin Peng, Pieter Abbeel, Sergey Levine, and Michiel van de Panne. Deepmimic: Example-guided deep reinforcement learning of physics-based character skills. *ACM Transactions on Graphics (TOG)*, 37(4):1–14, 2018.
- [6] Xue Bin Peng, Angjoo Kanazawa, Jitendra Malik, Pieter Abbeel, and Sergey Levine. Sfv: Reinforcement learning of physical skills from videos. *ACM Transactions on Graphics*, 2018.
- [7] Aravind Rajeswaran, Vikash Kumar, Abhishek Gupta, Giulia Vezzani, John Schulman, Emanuel Todorov, and Sergey Levine. Learning complex dexterous manipulation with deep reinforcement learning and demonstrations. In *Robotics: Science and Systems*, 2018.
- [8] Jie Tan, Tingnan Zhang, Erwin Coumans, Atil Iscen, Yunfei Bai, Danijar Hafner, Steven Bohez, and Vincent Vanhoucke. Sim-to-real: Learning agile locomotion for quadruped robots. In *Robotics: Science and Systems*, 2018.
- [9] John Schulman, Filip Wolski, Prafulla Dhariwal, Alec Radford, and Oleg Klimov. Proximal policy optimization algorithms. *arXiv preprint arXiv:1707.06347*, 2017.
- [10] John Schulman, Sergey Levine, Pieter Abbeel, Michael Jordan, and Philipp Moritz. Trust region policy optimization. In *International Conference on Machine Learning*, pages 1889–1897, 2015.
- [11] Volodymyr Mnih, Adria Puigdomenech Badia, Mehdi Mirza, Alex Graves, Timothy Lillicrap, Tim Harley, David Silver, and Koray Kavukcuoglu. Asynchronous methods for deep reinforcement learning. In *International conference on machine learning*, pages 1928–1937, 2016.
- [12] Nicolas Heess, Gregory Wayne, David Silver, Timothy Lillicrap, Tom Erez, and Yuval Tassa. Learning continuous control policies by stochastic value gradients. In *Advances in Neural Information Processing Systems*, pages 2944–2952, 2015.
- [13] Yan Duan, Xi Chen, Rein Houthooft, John Schulman, and Pieter Abbeel. Benchmarking deep reinforcement learning for continuous control. In *International Conference on Machine Learning*, pages 1329–1338, 2016.
- [14] Tuomas Haarnoja, Haoran Tang, Pieter Abbeel, and Sergey Levine. Reinforcement learning with deep energy-based policies. In *International Conference on Machine Learning*, pages 1352–1361, 2017.
- [15] Carlos Florensa, Yan Duan, and Pieter Abbeel. Stochastic neural networks for hierarchical reinforcement learning. *arXiv preprint arXiv:1704.03012*, 2017.
- [16] Xue Bin Peng, Glen Berseth, KangKang Yin, and Michiel Van De Panne. Deeploco: Dynamic locomotion skills using hierarchical deep reinforcement learning. *ACM Transactions on Graphics (TOG)*, 36(4):1–13, 2017.
- [17] Kevin Frans, Jonathan Ho, Xi Chen, Pieter Abbeel, and John Schulman. Meta learning shared hierarchies. *arXiv preprint arXiv:1710.09767*, 2017.
- [18] Ofir Nachum, Shixiang Shane Gu, Honglak Lee, and Sergey Levine. Data-efficient hierarchical reinforcement learning. In *Advances in Neural Information Processing Systems*, pages 3303–3313, 2018.
- [19] Konrad Rawlik, Marc Toussaint, and Sethu Vijayakumar. On stochastic optimal control and reinforcement learning by approximate inference. In *Robotics: Science and Systems*, 2013.
- [20] Brendan O’Donoghue, Remi Munos, Koray Kavukcuoglu, and Volodymyr Mnih. Combining policy gradient and q-learning. *arXiv preprint arXiv:1611.01626*, 2016.
- [21] John Schulman, Xi Chen, and Pieter Abbeel. Equivalence between policy gradients and soft q-learning. *arXiv preprint arXiv:1704.06440*, 2017.
- [22] Ofir Nachum, Mohammad Norouzi, Kelvin Xu, and Dale Schuurmans. Bridging the gap between value and policy based reinforcement learning. In *Advances in Neural Information Processing Systems*, pages 2775–2785, 2017.

- [23] Tuomas Haarnoja, Aurick Zhou, Pieter Abbeel, and Sergey Levine. Soft actor-critic: Off-policy maximum entropy deep reinforcement learning with a stochastic actor. *arXiv preprint arXiv:1801.01290*, 2018.
- [24] Tuomas Haarnoja, Aurick Zhou, Kristian Hartikainen, George Tucker, Sehoon Ha, Jie Tan, Vikash Kumar, Henry Zhu, Abhishek Gupta, Pieter Abbeel, et al. Soft actor-critic algorithms and applications. *arXiv preprint arXiv:1812.05905*, 2018.
- [25] OpenAI: Marcin Andrychowicz, Bowen Baker, Maciek Chociej, Rafal Jozefowicz, Bob McGrew, Jakub Pachocki, Arthur Petron, Matthias Plappert, Glenn Powell, Alex Ray, et al. Learning dexterous in-hand manipulation. *The International Journal of Robotics Research*, 39(1):3–20, 2020.
- [26] Wojciech Jaśkowski, Odd Rune Lykkebø, Nihat Engin Toklu, Florian Triffterer, Zdeněk Buk, Jan Koutník, and Faustino Gomez. Reinforcement learning to run... fast. In *The NIPS'17 Competition: Building Intelligent Systems*, pages 155–167. Springer, 2018.
- [27] Yunhao Tang and Shipra Agrawal. Discretizing continuous action space for on-policy optimization. *arXiv preprint arXiv:1901.10500*, 2019.
- [28] Lasse Espeholt, Hubert Soyer, Remi Munos, Karen Simonyan, Volodymyr Mnih, Tom Ward, Yotam Doron, Vlad Firoiu, Tim Harley, Iain Dunning, et al. Impala: Scalable distributed deep-rl with importance weighted actor-learner architectures. *arXiv preprint arXiv:1802.01561*, 2018.
- [29] Richard S Sutton, David A McAllester, Satinder P Singh, and Yishay Mansour. Policy gradient methods for reinforcement learning with function approximation. In *Advances in neural information processing systems*, pages 1057–1063, 2000.
- [30] John Schulman, Philipp Moritz, Sergey Levine, Michael Jordan, and Pieter Abbeel. High-dimensional continuous control using generalized advantage estimation. *arXiv preprint arXiv:1506.02438*, 2015.
- [31] David Silver, Guy Lever, Nicolas Heess, Thomas Degris, Daan Wierstra, and Martin Riedmiller. Deterministic policy gradient algorithms. In *International Conference on Machine Learning*, pages 387–395, 2014.
- [32] Arnaud Doucet, Nando De Freitas, and Neil Gordon. An introduction to sequential monte carlo methods. In *Sequential Monte Carlo methods in practice*, pages 3–14. Springer, 2001.
- [33] Adrian FM Smith and Alan E Gelfand. Bayesian statistics without tears: a sampling–resampling perspective. *The American Statistician*, 46(2):84–88, 1992.
- [34] Neil J Gordon, David J Salmond, and Adrian FM Smith. Novel approach to nonlinear/non-Gaussian Bayesian state estimation. *IEE proceedings F (radar and signal processing)*, 140(2):107–113, 1993.
- [35] Genshiro Kitagawa. Monte Carlo filtering and smoothing method for non-Gaussian nonlinear state space model. *Inst. Statist. Math. Res. Memo.*, 1993.
- [36] Marco F Huber, Tim Bailey, Hugh Durrant-Whyte, and Uwe D Hanebeck. On entropy approximation for gaussian mixture random vectors. In *2008 IEEE International Conference on Multisensor Fusion and Integration for Intelligent Systems*, pages 181–188. IEEE, 2008.
- [37] Augustine Kong, Jun S Liu, and Wing Hung Wong. Sequential imputations and bayesian missing data problems. *Journal of the American statistical association*, 89(425):278–288, 1994.
- [38] Eric Jang, Shixiang Gu, and Ben Poole. Categorical reparameterization with gumbel-softmax. *arXiv preprint arXiv:1611.01144*, 2016.
- [39] Chris J Maddison, Andriy Mnih, and Yee Whye Teh. The concrete distribution: A continuous relaxation of discrete random variables. *arXiv preprint arXiv:1611.00712*, 2016.
- [40] Eric Jang, Shixiang Gu, and Ben Poole. Categorical reparameterization with gumbel-softmax. In *International Conference on Learning Representations (ICLR 2017)*, 2017.
- [41] Luke Metz, Julian Ibarz, Navdeep Jaitly, and James Davidson. Discrete sequential prediction of continuous actions for deep rl. *arXiv preprint arXiv:1705.05035*, 2017.
- [42] Minjae Kang, Kyungjae Lee, and Songhwai Oh. Soft action particle deep reinforcement learning for a continuous action space. In *2019 IEEE/RSJ International Conference on Intelligent Robots and Systems (IROS)*, pages 5028–5033. IEEE, 2019.
- [43] Greg Brockman, Vicki Cheung, Ludwig Pettersson, Jonas Schneider, John Schulman, Jie Tang, and Wojciech Zaremba. Openai gym. *arXiv preprint arXiv:1606.01540*, 2016.
- [44] Jie Tan, Karen Liu, and Greg Turk. Stable proportional-derivative controllers. *IEEE Computer Graphics and Applications*, 31(4):34–44, 2011.

- [45] P Del Moral, A Doucet, and A Jasra. On adaptive resampling procedures for sequential monte carlo methods. *Bernoulli*, 18(1):252–278, 2012.
- [46] Diederik P Kingma and Jimmy Ba. Adam: A method for stochastic optimization. *arXiv preprint arXiv:1412.6980*, 2014.
- [47] Andrew M Saxe, James L McClelland, and Surya Ganguli. Exact solutions to the nonlinear dynamics of learning in deep linear neural networks. *arXiv preprint arXiv:1312.6120*, 2013.

Appendices

A Particle Filter

While different particle filtering approaches exist in the literature, here we focus on the sequential importance resampling (SIR) approach [33, 34]. SIR is a Monte Carlo method that can be used to estimate the posterior distribution of the states, \mathbf{x} , of some Markov process through sampling. More specifically, given the observations $\mathbf{z}_{0:t}$, SIR approximates the posterior distributions $p(\mathbf{x}_t|\mathbf{z}_{0:t})$ at time step t by a weighted set of N particles $\{\langle \mathbf{x}_t^{(i)}, w_t^{(i)} \rangle, i \in [1, N]\}$:

$$p(\mathbf{x}_t|\mathbf{z}_{0:t}) \approx \sum_i w_t^{(i)} \delta(\mathbf{x}_t, \mathbf{x}_t^{(i)}), \quad (18)$$

where $\delta(\cdot)$ is the Dirac delta function, $\mathbf{x}_t^{(i)}$ denotes the state of the i -th particle, $w_t^{(i)}$ its weight, and $\sum_i w_t^{(i)} = 1$.

Particles are usually initialized with equal weights and obtained by drawing from a priori distribution $p(\mathbf{x}_0)$, which may be a uniform distribution if there is a lack of a priori knowledge of the distribution. Then at each time step, given the observation \mathbf{z}_t , the posterior density is computed in three steps:

1. *Update*: N new samples are generated from the previous particle configuration

$$\mathbf{x}_t^{(i)} \sim q(\mathbf{x}_t|\mathbf{x}_{t-1}^{(i)}, \mathbf{z}_t) \quad (19)$$

where $q(\cdot)$ denotes the importance distribution. In many problems, the dynamics model is used as the importance distribution, i.e. $q(\mathbf{x}_t|\mathbf{x}_{t-1}^{(i)}, \mathbf{z}_t) = p(\mathbf{x}_t|\mathbf{x}_{t-1}, \mathbf{u}_{t-1})$ for some control input \mathbf{u} , which greatly simplifies the iterative estimation process.

2. *Prediction*: The weights of the particles are updated as

$$w_t^{(i)} \propto w_{t-1}^{(i)} \frac{p(\mathbf{z}_t|\mathbf{x}_t^{(i)})p(\mathbf{x}_t^{(i)}|\mathbf{x}_{t-1}^{(i)}, \mathbf{u}_{t-1})}{q(\mathbf{x}_t^{(i)}|\mathbf{x}_{t-1}^{(i)}, \mathbf{z}_t)}, \quad (20)$$

and then normalized to sum to unity.

3. *Resampling*: It can be shown that the variance of the weights increases at every time step. Therefore, the above two steps will converge to a situation that all but one particle have weights that are zero or close to zero [37]. To avoid this problem of degeneracy, resampling can be performed, where N new samples are drawn with replacement from the current set of particles based on the weights. The new samples are then used to replace the current set, with all particles resetting their weights to $1/N$. While resampling can be performed at every step, the variance of the particle set as a true estimator of the posterior distribution increases. Common strategies to avoid this issue, is to perform resampling every fixed number of steps, or when the effective number of particles is too low [45].

Connection between SIR and PFPN. Similar to a particle filter that estimates the posterior density $p(\mathbf{x}_t|\mathbf{z}_{0:t})$ based on the observations $\mathbf{z}_{0:t}$, our approach aims at estimating the action policy $p(\mathbf{a}_t|\mathbf{z}_{0:t})$ by exploiting sampled state-action-reward experiences, i.e.

$$\mathbf{z}_t := \langle \mathbf{s}_t, \mathbf{a}_t, r_t \rangle. \quad (21)$$

In our case, the estimation process is performed by Equation 5 using a set of particles per action dimension:

$$\mathbf{x}_t := \{\langle \mu_i, \sigma_i \rangle\}, \quad (22)$$

where each particle, i , represents a univariate Gaussian distribution and has an associated weight $w_i(\mathbf{s}_t|\theta)$. In Equation 5, $p_i(a_t|\mu_i, \sigma_i)$ directly gives us a measurement between a_t and the particle located at μ_i that has a similar function with $\delta(\cdot, \cdot)$ in Equation 18.

In analogy with the formal SIR process outlined above, our approach has three main phases. In the *Update* phase, we update each particle using Equation 8, where the transition prior probability distribution is used as importance function q and A_t can be considered as the control signal \mathbf{u}_t . In the *Prediction* phase, we update the weight of each particle using Equation 9 based on the likelihood

$$p(\mathbf{z}_t|\mathbf{x}_t^{(i)}) := p_i(a_t|\mu_i, \sigma_i). \quad (23)$$

To address the problem of particle degeneracy, in the *Resampling* phase we replace particles that have small weights by sampling from the current set of particles using Equation 12.

A key difference between PFPN and SIR is that weights in PFPN are state-dependent while a particle filter considers only the current state. Consequently, in the resampling phase of PFPN, we do not resample the entire set of particles but only degenerate ones. If a new set of particles would have been generated instead, equalizing the weights after resampling would have prevented us from tracing and exploiting interesting particles defined for a given state.

B Logits Correction when Equalizing Weights during Resampling

The weight for the i -th particle is achieved by softmax operation, which is applied to the unnormalized logits, i.e. the direct output of the policy network, L_i :

$$w_i(s_t) = \text{SOFTMAX}(L_i(s_t)) = \frac{e^{L_i(s_t)}}{\sum_k e^{L_k(s_t)}}. \quad (24)$$

Suppose that a set of dead particles \mathcal{D}_τ duplicates a target particle τ sampled using Equation 12. Particles in $\mathcal{D}_\tau \cup \{\tau\}$ will share the same logits L'_τ after resampling, and thus have the same weights. In order to ensure that the introduction of L'_τ will not influence the weight of particles that are not in $\mathcal{D}_\tau \cup \{\tau\}$, the exponential sum of logits must be identical before and after resampling, i.e.

$$\sum_k e^{L_k(s_t)} = \sum_{\mathcal{D}_\tau \cup \{\tau\}} e^{L'_\tau(s_t)} + \sum_{k \notin \mathcal{D}_\tau \cup \{\tau\}} e^{L_k(s_t)}. \quad (25)$$

Equation 25 can be rewritten as

$$\sum_{s \in \mathcal{D}_\tau} e^{L_s(s_t)} + e^{L_\tau(s_t)} = (|\mathcal{D}_\tau| + 1)e^{L'_\tau(s_t)}, \quad (26)$$

where $\tau \notin \mathcal{D}_k$ for any dead particle set \mathcal{D}_k , i.e. a target particle will not be tagged as dead at all, since a target particle is drawn according to the particles' weights and since dead particles are defined as the ones having too small or zero weight to be chosen.

Given that $e^{L_s(s_t)} \approx 0$ for any dead particle $s \in \mathcal{D}_\tau$ and that the number of particles is limited, it holds

$$e^{L_\tau} \approx (|\mathcal{D}_\tau| + 1)e^{L'_\tau(s_t)}. \quad (27)$$

Taking the logarithm of both sides of the equation leads to

$$L'_\tau(s_t) \approx L_\tau(s_t) - \log(|\mathcal{D}_\tau| + 1). \quad (28)$$

Therefore, after copying the neural network parameters, $\omega_{\cdot, \tau}$ and b_τ , who generate $L_\tau(s_t)$, to the parameters of the dead particles $\omega_{\cdot, s}$ and b_s where $s \in \mathcal{D}_\tau$, a correction term $-\log(|\mathcal{D}_\tau| + 1)$ should be applied for all particles in $\mathcal{D} \cup \tau$, as Equation 15, to ensure that the policy distribution after resampling changes trivially.

If we perform random sampling not based on the weights during resampling (see Appendix E), it is possible to pick a dead particle as the target particle. In that case

$$L'_\tau(s_t) \approx L_\tau(s_t) - \log(|\mathcal{D}_\tau| + (1 - \sum_k \delta(\tau, \mathcal{D}_k))), \quad (29)$$

where $L'_\tau(s_t)$ is the new logits shared by particles in \mathcal{D}_τ and $\delta(\tau, \mathcal{D}_k)$ is the Kronecker delta function

$$\delta(\tau, \mathcal{D}_k) = \begin{cases} 1 & \text{if } \tau \in \mathcal{D}_k \\ 0 & \text{otherwise} \end{cases} \quad (30)$$

that satisfies $\sum_k \delta(\tau, \mathcal{D}_k) \leq 1$. Then, for the particle τ , its new logits can be defined as

$$L''_\tau(s_t) \approx (1 - \sum_k \delta(\tau, \mathcal{D}_k))L'_\tau(s_t) + \sum_k \delta(\tau, \mathcal{D}_k)L_\tau. \quad (31)$$

Consequently, the target particle τ may or may not share the same logits with those in \mathcal{D}_τ , depending on if it is tagged as dead or not.

C Hyperparameters

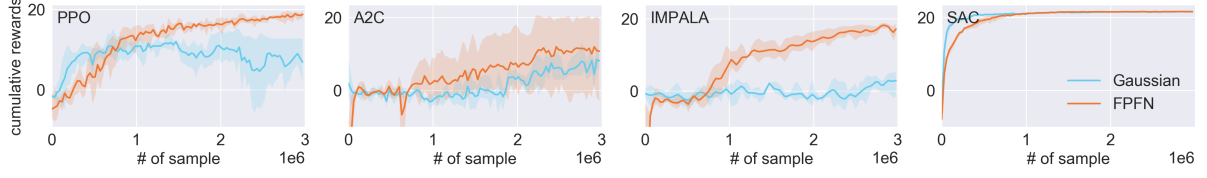
Table 2 lists the default hyperparameters used in all of our experiments. Regarding PPO and A2C, in all Roboschool tasks except for the HumanoidBulletEnv-v0 one, we use the Generalized Advantage Estimation (GAE) and a single worker thread; for HumanoidBulletEnv-v0 and DeepMimic tasks, we exploit the advantage of distributed training and used DPPO (synchronous PPO) and A3C (asynchronous A2C) with multiple worker threads, while IMPALA is natively multi-thread. Differentiable entropy is employed in A2C/A3C and IMPALA cases to stabilize the training, where PFPN uses the entropy of the categorical distribution, through which Gaussians represented by particles are mixed, as it is described in Section 3.1.

Besides the number of particles, given an algorithm, the hyperparameters used for PFPN and the corresponding Gaussian policy cases are identical. Two hyperparameters for PFPN only are the resampling interval and dead particle detection threshold. The resampling interval is set to be 25 environment episodes considering the number of worker threads. The dead particle detection threshold is set dynamically depending on the number of particles. See Appendix E for the details about the sensitivity of PFPN to these two hyperparameters.

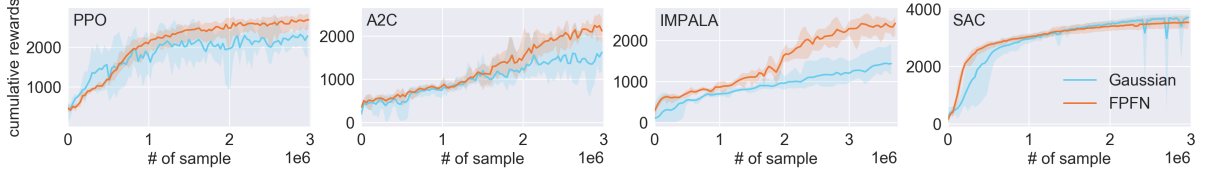
Parameter	Value
<i>Shared</i>	
optimizer	Adam [46]
activation function	ReLU
resampling interval	25 environment episodes per worker thread
dead particle detection threshold (ϵ)	0.05/number of particles per action dimension
clip range (PPO/DPPO)	0.2
GAE discount factor (PPO/DPPO, A2C/A3C, λ)	0.95
truncation level (IMPALA, \bar{c} , $\bar{\rho}$)	1.0
reply buffer size (SAC)	$1 \cdot 10^6$
<i>Roboschool Environments</i>	
learning rate	$3 \cdot 10^{-4}$
weight initializer	Orthogonal [47]
number of neurons in hidden layers	[256, 256]
number of particle per action dimension	35
discount factor (γ)	0.99
mini batch size (PPO)	128
mini batch size (DPPO, <i>Humanoid</i>)	128×8 worker threads
mini batch size (A2C)	32
mini batch size (A3C, <i>Humanoid</i>)	32 (16 worker threads)
mini batch size (IMPALA)	32×2 (8 actor threads in total)
mini batch size (IMPALA, <i>Humanoid</i>)	64×4 (32 actor threads in total)
mini batch size (SAC)	256
unroll length (PPO/DPPO)	2048
coefficient of policy entropy loss term (A2C/A3C, IMPALA)	0.01
<i>DeepMimic Environments</i>	
learning rate	$1 \cdot 10^{-4}$
weight initializer	Truncated Normal with standard deviation of 0.01
number of neurons in hidden layers	[1024, 512]
number of particle per action dimension	100
discount factor (γ)	0.95
mini batch size (DPPO)	32×8 worker threads
mini batch size (A3C)	32 (16 worker threads)
mini batch size (IMPALA)	64×4 (32 actor threads in total)
mini batch size (SAC)	256
unroll length (DPPO)	512
coefficient of policy entropy loss term (A3C, IMPALA)	0.00025

Table 2: Default Hyperparameters in Baseline Benchmarks

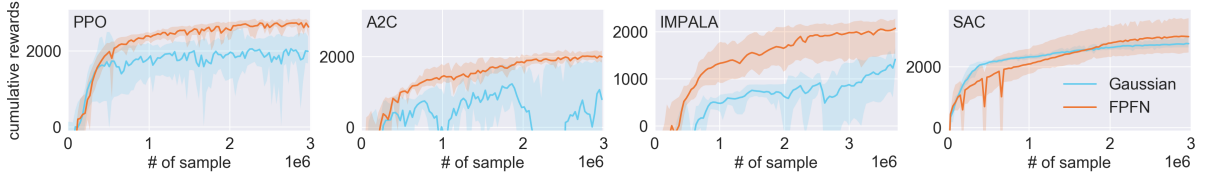
D Additional Results



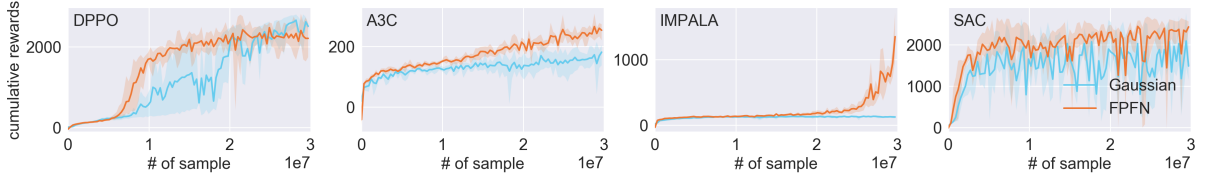
(a) ReacherBulletEnv-v0



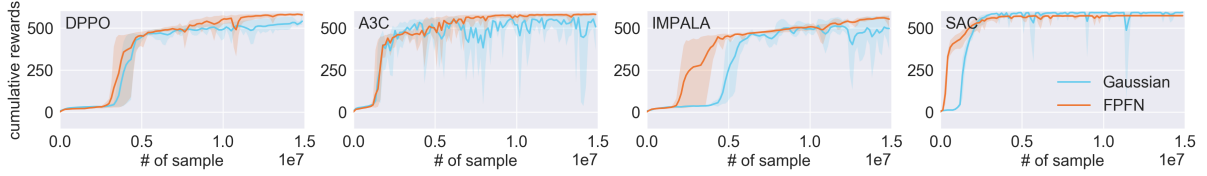
(b) AntBulletEnv-v0



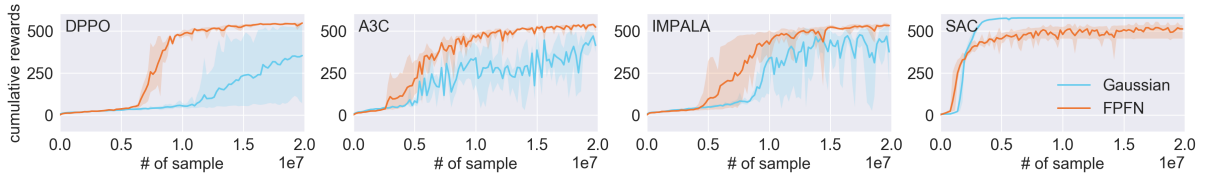
(c) HalfCheetahBulletEnv-v0



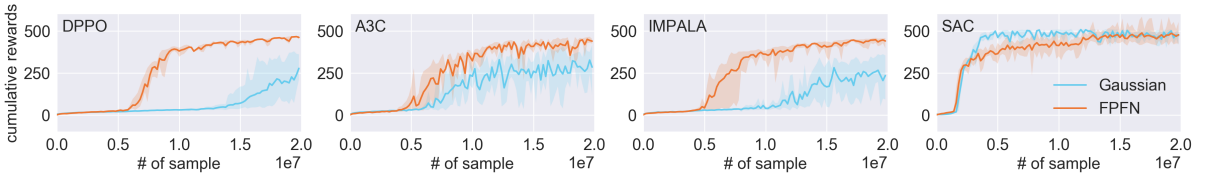
(d) HumanoidBulletEnv-v0



(e) DeepMimicWalk



(f) DeepMimicPunch



(g) DeepMimicKick

Figure 3: Training curves on continuous control tasks from the Roboschool and DeepMimic environments.

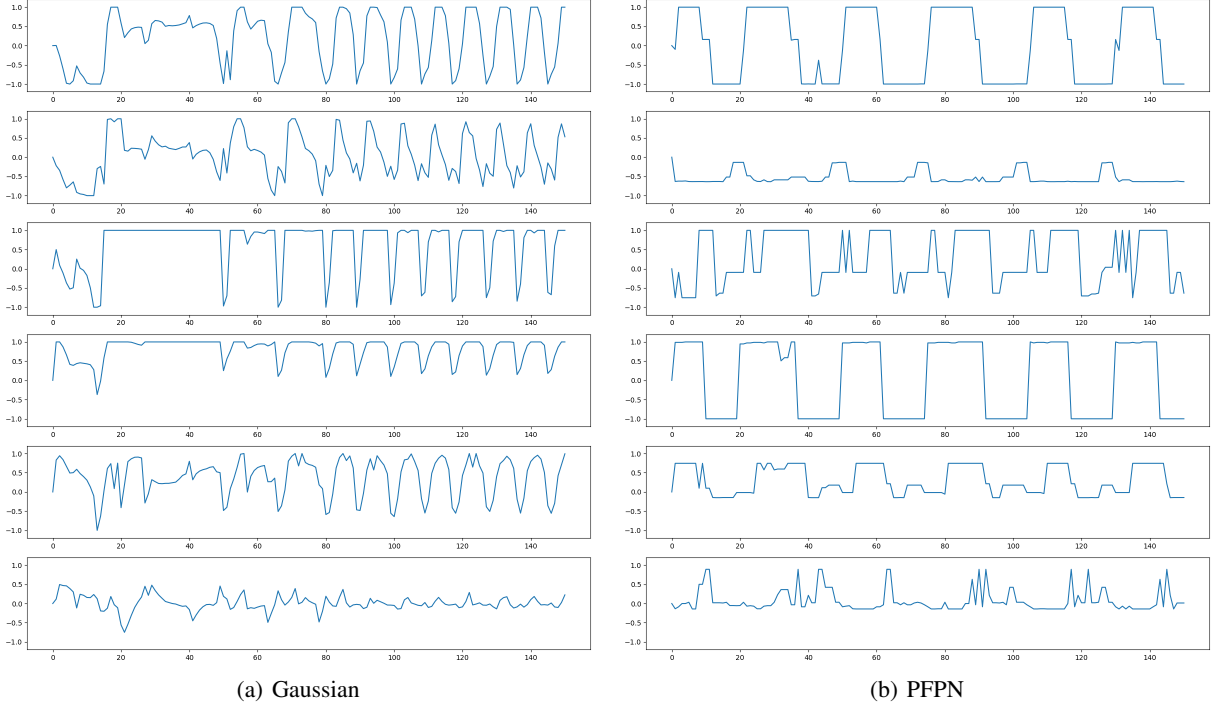


Figure 4: Torque patterns generated by Gaussian-based A2C and PFPN-A2C on HalfCheetahBulletEnv-v0. Each row denotes the corresponding policy per action dimension executed for 150 steps. Torque values are normalized to lie between -1 and 1. For each action dimension, PFPN generates significantly different torque profiles than the ones obtained by Gaussian A2C both in terms of frequency and/or amplitude that result in higher asymptotic performance (shown in Figure 3).

Figure 3 compares baselines that employ Gaussian policies to their PFPN counterparts on a variety of Roboschool and DeepMimic tasks. The results are obtained as discussed in Section 5.1, where ten evaluation trials run every 1,000 training steps using deterministic actions. In most tasks, PFPN outperforms the default Gaussian PPO/DPPO, A2C/A3C, and IMPALA baselines and is more stable across different training trials. Additionally, given the state-of-the-art performance of SAC, the PFPN version of SAC performs comparably to the vanilla SAC baseline in the Roboschool tasks. In DeepMimic tasks, PFPN-based SAC has faster convergence, though it exhibits slightly worse final performance.

We note that due to its highly scalable nature, IMPALA is particularly suited for fast training of complex tasks, as we can take advantage of distributed learning and significantly reduce the computational cost in terms of absolute wall clock time. In DeepMimic tasks, for example, although the final performance of IMPALA cannot reach the performance of SAC, IMPALA with 15 millions of samples takes about four hours using 32 actor threads during our tests. In contrast, SAC requires more than seven hours to reach the same performance and more than one day to reach the same number of samples. Overall, our PFPN implementation of IMPALA can significantly increase the performance and speed of convergence of the default baseline and can provide performance comparable to that of SAC.

To further highlight the value that particle-based discretization adds to the action exploration problem, we also compare the torques generated by a PFPN-A2C policy in the HalfCheetahBulletEnv-v0 task to the ones obtained by vanilla A2C with Gaussian action policy. As it can be seen in Figure 4, there is a significant difference in the controls taken by the two agents, with PFPN leading to higher performance as shown in Figure 3.

E Resampling

E.1 Strategies

We tested PFPN with the default resampling strategy explained in Section 3.3, where a target particle is selected with a probability proportional to its weights, against a number of alternative strategies where a dead particle resamples

randomly from the top- $x\%$ of particles as ranked by their weights. Table 3 highlights the corresponding results from which it is evident that the default resampling strategy compares favorably to the other strategies in terms of both mean performance and variance.

	# of samples	PFPN	Top-0%	Top-1%	Top-50%	Top-100%
AntBulletEnv-v0 PPO	1.0e6	2085 \pm 174	2229 \pm 223	2227 \pm 189	2081 \pm 238	2212 \pm 166
	2.0e6	2487 \pm 247	2587 \pm 210	2445 \pm 242	2581 \pm 192	2670 \pm 167
	3.0e6	2714 \pm 124	2630 \pm 156	2684 \pm 231	2697 \pm 228	2855 \pm 205
HalfCheetahBulletEnv-v0 PPO	1.0e6	2370 \pm 110	2207 \pm 169	2350 \pm 249	2536 \pm 87	2432 \pm 31
	2.0e6	2443 \pm 191	2273 \pm 117	2740 \pm 52	2759 \pm 43	2699 \pm 32
	3.0e6	2764 \pm 68	2548 \pm 306	2834 \pm 40	2669 \pm 218	2794 \pm 53
HumanoidBulletEnv-v0 DPPO	1.0e7	1647 \pm 187	954 \pm 675	1160 \pm 530	1656 \pm 132	1672 \pm 395
	2.0e7	2207 \pm 107	2375 \pm 364	2277 \pm 158	2201 \pm 169	2245 \pm 98
	3.0e7	2444 \pm 207	2555 \pm 254	2041 \pm 707	2191 \pm 106	1846 \pm 318
DeepMimicWalk DPPO	0.5e7	453 \pm 32	267 \pm 159	455 \pm 14	174 \pm 159	290 \pm 166
	1.0e7	554 \pm 18	471 \pm 44	550 \pm 18	514 \pm 17	529 \pm 17
	1.5e7	583 \pm 3	517 \pm 33	583 \pm 5	572 \pm 10	577 \pm 8
DeepMimicWalk IMPALA	0.5e7	450 \pm 14	448 \pm 18	448 \pm 16	349 \pm 116	454 \pm 18
	1.0e7	508 \pm 12	487 \pm 20	511 \pm 25	504 \pm 11	506 \pm 11
	1.5e7	563 \pm 6	539 \pm 11	559 \pm 13	562 \pm 7	563 \pm 7

Table 3: Comparison between the default PFPN strategy and Top- $x\%$ resampling strategies on different Roboschool and DeepMimic tasks. Reported numbers denote the average cumulative reward of evaluation rollouts at the steps when a certain number of samples have been exploited \pm the standard deviation. Although the default strategy does not always achieve the best final performance in all benchmarks, overall it is more stable and results in higher performance.

E.2 Hyperparameters

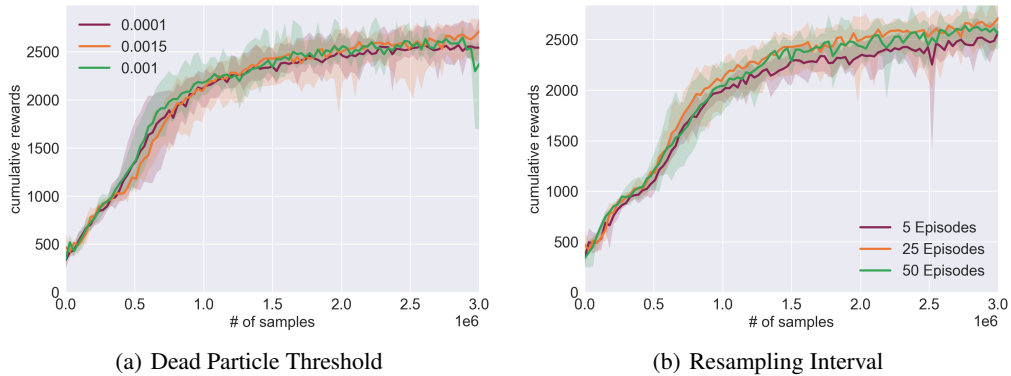


Figure 5: Sensitivity of PFPN to resampling hyperparameters on the AntBulletEnv-v0 task using PPO with 35 particles for each action dimension. The resampling process itself is robust and not very sensitive to the dead particle threshold ϵ and the resampling frequency, since particles are movable and their locations can be further optimized after resampling. However, there still should be some interval between resampling operations to allow for enough steps to optimize the distribution of particles. Too small of a resampling interval, 5 episodes in the figure, can hurt the performance.

Our default resampling strategy has two hyperparameters to tune: the threshold, ϵ , which determines whether a particle is not active anymore and needs to be revived (see Equation 11), and the resampling frequency, i.e. the number of environment steps as the interval between resampling. In practice, we found a small value of ϵ below 0.01 to work quite well for all baselines and tasks as shown in Figure 5. In our comparative evaluations in Figures 1 and 3, we set

the threshold dynamically as $0.05/n$, where n is the number of particles used for one action dimension. In addition, PFPN is quite robust in terms of the resampling frequency employed, with frequency values in the range from 25 to 50 environment episodes resulting in high performance in both Roboschool and DeepMimic benchmarks.

F Analysis of Adaptive Discretization

F.1 Sensitivity to Number of Particles

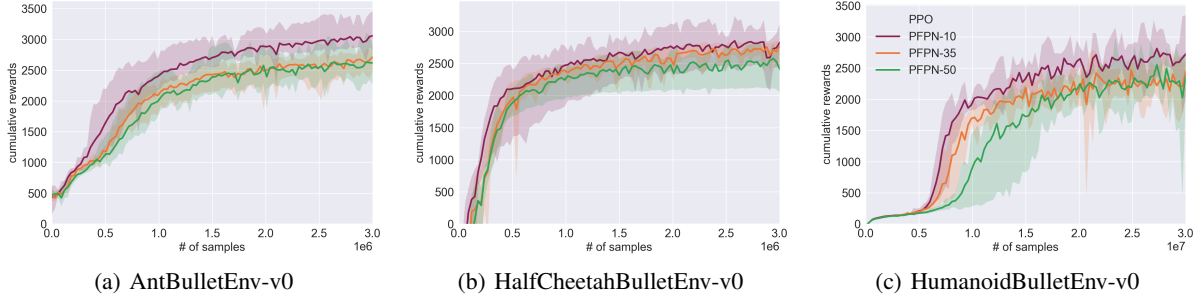


Figure 6: Performance of PFPN in Roboschool tasks using PPO/DPPO with a varying number of particles per action dimension.

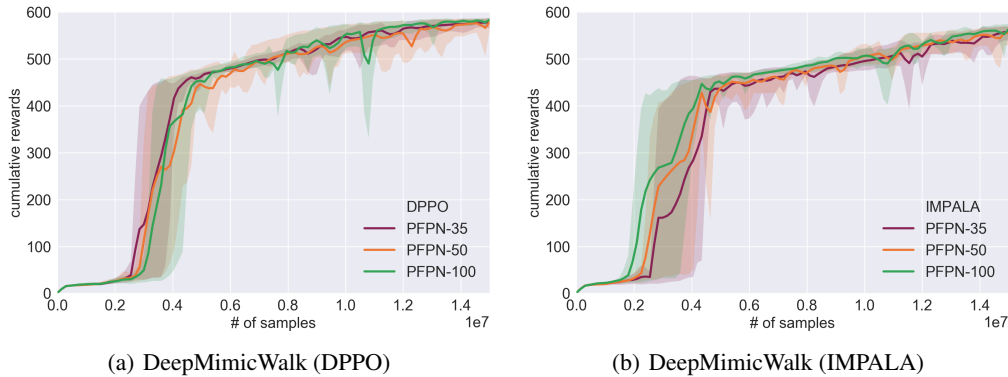


Figure 7: Performance of PFPN in the DeepMimicWalk task using DPPO and Impala while varying the number of particles per action dimension.

We show the sensitivity of PFPN to the number of particles in Figure 6 and 7. As can be seen, for each baseline and task, the best final performance is obtained by different number of particles. Despite this, though, we found that there is a wide range of particle numbers that works quite well in each task, outperforming the traditional Gaussian-based policy networks. Typical values are 10 and 35 particles for Roboschool tasks, with policies obtained with 10 particles per action dimension resulting in higher performance but also exhibiting more variance in some cases. In DeepMimic tasks, a higher number of particles is required, with 50 and 100 being the recommended values and the latter resulting in more stable policies across different trials.

# of samples		bins/particles					
		10		35		50	
		PFPN	DISCRETE	PFPN	DISCRETE	PFPN	DISCRETE
AntBulletEnv-v0 PPO	1e6	2394 ± 135	2377 ± 126	2085 ± 174	1838 ± 379	2000 ± 239	1693 ± 245
	2e6	2873 ± 129	2698 ± 200	2487 ± 247	2180 ± 310	2475 ± 269	2215 ± 207
	3e6	3059 ± 223	2935 ± 229	2714 ± 124	2498 ± 242	2617 ± 221	2416 ± 245
HalfCheetahBulletEnv-v0 PPO	1e6	2478 ± 311	2408 ± 241	2370 ± 110	2221 ± 86	2268 ± 156	2098 ± 205
	2e6	2745 ± 236	2535 ± 313	2443 ± 191	2391 ± 180	2372 ± 216	2407 ± 283
	3e6	2825 ± 208	2740 ± 391	2764 ± 68	2550 ± 84	2414 ± 281	2489 ± 250
HumanoidBulletEnv-v0 DPPO	1e7	1880 ± 83	1787 ± 179	1647 ± 187	295 ± 33	883 ± 382	238 ± 12
	2e7	2598 ± 201	2110 ± 547	2207 ± 107	2093 ± 417	2058 ± 289	1739 ± 125
	3e7	2725 ± 505	2372 ± 96	2444 ± 207	2075 ± 570	2369 ± 263	2172 ± 250
# of samples		35		50		100	
		PFPN	DISCRETE	PFPN	DISCRETE	PFPN	DISCRETE
DeepMimicWalk DPPO	0.5e7	463 ± 10	152 ± 158	445 ± 29	333 ± 113	453 ± 32	108 ± 147
	1.0e7	548 ± 16	291 ± 148	536 ± 20	481 ± 37	554 ± 18	386 ± 149
	1.5e7	578 ± 7	384 ± 178	566 ± 30	517 ± 38	583 ± 3	472 ± 64
DeepMimicWalk IMPALA	0.5e7	435 ± 30	274 ± 135	437 ± 21	142 ± 147	450 ± 14	149 ± 155
	1.0e7	496 ± 17	273 ± 163	507 ± 17	355 ± 127	508 ± 12	271 ± 146
	1.5e7	557 ± 11	375 ± 169	545 ± 34	454 ± 20	563 ± 6	372 ± 87

Table 4: Comparison between PFPN and uniform discretization (DISCRETE) while varying the resolution (number of particles and number of bins, respectively) of each action dimension. For PFPN the default resampling strategy is employed. In all tasks, PFPN outperforms DISCRETE for a given resolution, with the differences being more apparent as the task complexity increases. In addition, PFPN’s performance remains quite stable across different resolutions and tasks.

F.2 Comparison to Uniform Discretization

In Table 4, we also compare PFPN to a uniform discretization scheme where each action dimension is divided into a number of equally sized bins before training and actions are learned from a categorical distribution over those bins (see, e.g. [27]). As can be seen our adaptive, particle-based, discretization scheme exhibits similar or significantly better performance than the uniform one for a given task and action resolution, while being more stable.

The value of our adaptive scheme is also evident by the final distribution of particles as shown in Figure 8 for the HalfCheetahBulletEnv-v0 task. Discrete actions defined by the particle locations are adaptively changed during training. They converge to relatively optimal regions and improve the performance by increasing the resolution of those regions, while the performance of fixed discretization depends on the location of the discretized actions which are usually chosen uniformly as well as blindly to some degree. In DeepMimic tasks, where the action space consists of a set of 4D axis-angles, the interesting action space is often located into a narrow region (see, e.g. Figure 9). In such scenarios, the problem of employing uniform, fixed discretization becomes even more apparent, since many of the discretized actions may be placed in low-reward regions and thus a fine resolution is needed to capture the interesting action space.

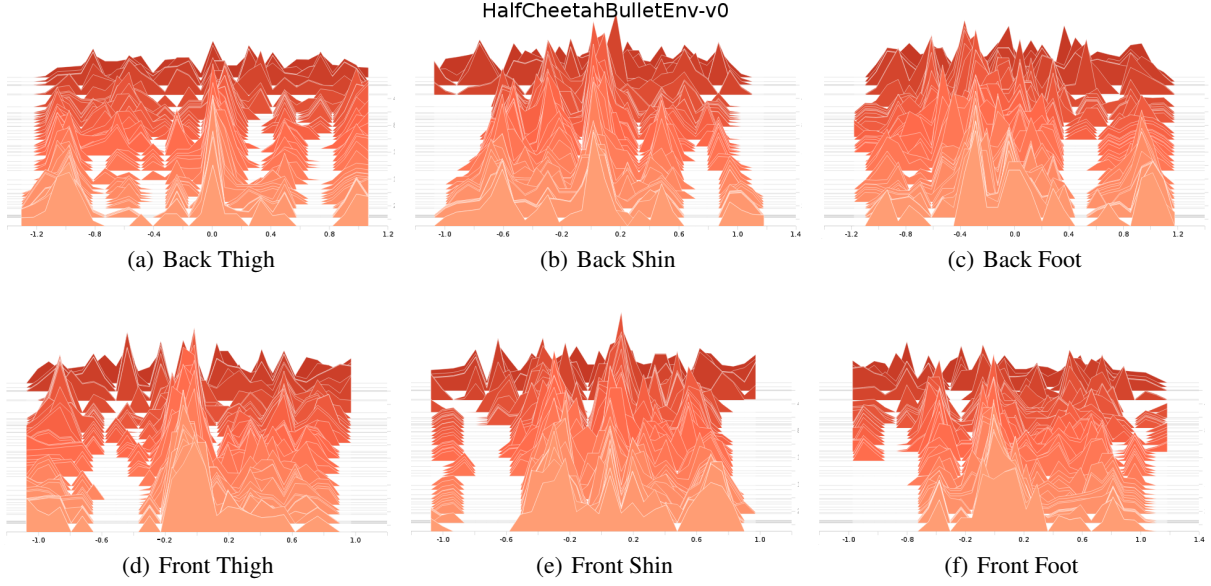


Figure 8: Evolution of particle distribution per action dimension during training for the HalfCheetahBulletEnv-v0 task using PPO. The x-axis denotes normalized action values and the y-axis the number of particles assigned to each region. Particles are initially distributed uniformly along a dimension (dark colors) and their locations adaptively change as the policy network is trained (light colors). This allows PFPN to put emphasis on interesting locations and capture the multimodality of the action space, as opposed to fixed discretization schemes where the final performance heavily relies on the choice of initial candidate locations to find a good solution.

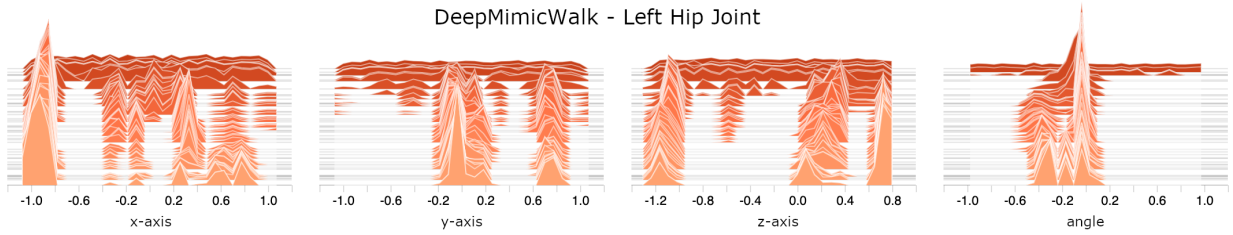


Figure 9: Particle distribution evolution of the four action dimensions for the left hip joint in DeepMimicWalk task using DPPO. Given a task, the valid movement range of the joint may be restrained only in some small ranges, while the action space covers the entire movement range of the joint. Compared to uniform discretization that would place many discrete, candidate actions in bad regions, our adaptive discretization approach can exploit all candidate actions effectively.